Finite Element Analysis and in Vitro Biomechanical Experiment on the Effect of Unilateral Partial Facetectomy Performed by Percutaneous Endoscopy on the Stability of Lumbar Spine

Xin-ru Li
Dalian Medical University
Zi-tong Li
Dalian Medical University
Lu-ming Nong (tessys2008@163.com)
The Affiliated Changzhou No.2 People's Hospital of Nanjing Medical University https://orcid.org/0000-0002-4265-3435

Research article

Keywords: Biomechanics, Bioengineering, Preclinical Studies, Therapeutics, Unilateral Partial Facetectomy

Posted Date: February 1st, 2021

DOI: https://doi.org/10.21203/rs.3.rs-170544/v1

Abstract

Purpose: To investigate the lumbar biomechanical effects of unilateral partial facetectomy (UPF) of different facet joint (FJ) portions under percutaneous endoscopy.

Methods: A 3D finite element (FE) model of the lumbar spine and 40 fresh calf spine models were used to simulate UPF under a physiological load performed through 3 commonly used needle insertion points (IPs) : (1) The apex of the superior FJ (as the first IP), (2) The midpoint of the ventral side of the superior FJ (as the second IP), (3) The lowest point of the ventral side of the superior FJ (as the third IP). The range of motion (ROM) and the L4/5 intradiscal maximum pressure (IMP) were measured and analyzed under a physiological load in all models during flexion, extension, left-right lateral flexion, and left-right axial rotation.

Results: When UPF was performed through the first and the third IPs, the ROM of the lumbar spine and the L4/5 IMP in the FE model were significantly increased compared with those in the intact FE model. When UPF was performed through the second IP, the ROM of the lumbar spine and the L4/5 IMP were not significantly different compared with those in the intact FE model. When UPF was performed through the second IP, the ROM of the lumbar spine and the L4/5 IMP in the calf spine models were not statistically different from the intact calf spine model.

Conclusion: UPF through the second IP resulted in a minimal impact on the biomechanics of the lumbar spine. Thus, it might be considered as the most appropriate IP for UPF.

Introduction

Lumbar instability often occurs after traditional open spinal surgery, leading to chronic pain in patients [1, 2]. Thanks to the development of minimally invasive technology, percutaneous endoscopic transforaminal discectomy (PETD) is widely used in clinical practice due to its advantages, such as less damage and fast recovery [3, 4]. However, PETD has its limitations. In order to effectively perform the endoscopic decompression and expand the working channel of the endoscope during the surgery, part of the bone structure of the superior facet joint (FJ) is often removed by facetectomy. Numerous studies showed that the integrity of the FJs is important to maintain the stability of the lumbar spine, since they are the main load-bearing structure of the spine [5–8]. The FJ can bear various forms of load such as compression, shear and axial rotation [9, 10]. However, when the FJ cartilage is damaged, the concentration of inflammatory mediators in the joint cavity increases, stimulating the nerve fiber endings in the FJ capsule, thus causing chronic pain in the FJs and accelerating their degeneration [11, 12]. Clinical studies revealed that some patients show lumbar instability after PETD [13–15], demonstrating that different methods of facetectomy have different effects on the stability of the lumbar spine. Biomechanical studies showed that the stability of the lumbar spine changes when more than 30% of the unilateral FJ is removed [16]. However, the method used for FJ resection in this study was not performed in the same way as it is performed in clinical practice, and the effect of resection of different FJ portions

on lumbar spine stability has not been studied yet. Therefore, this study used 3D finite element (FE) models and calf spine models to simulate unilateral partial facetectomy (UPF) performed by PETD technology to explore the best approach to remove the FJ to achieve an adequate decompression without causing lumbar instability.

Material And Methods

1. Development of the 3D FE Model

A healthy male volunteer (30 years old, height 175 cm, weight 70 kg) with no previous family history of lumbar disease was selected to participate to our experiment. After the exclusion of the presence of low back pain, lumbar deformity and other lumbar diseases in the volunteer, the informed consent form was signed, and a 3D computed tomography (CT) scan of the lumbar spine was performed (General Electric Company, Boston, Massachusetts, USA) to obtain the lumbar CT data. The high-resolution CT data were stored in DICOM (Digital Imaging and Communications in Medicine) format and imported into the Mimics 15.0 software (Materialise, Leuven, Belgium) to develop the L3-S1 3D geometric model. The model was imported into the 3-matic 7.0 software (Materialise), and its modeling tools were used to build a model of intervertebral discs and the upper and lower cartilage endplates. Then the mesh derivation function in Geomagic Studio 12.0 software (Geomagic, Raleigh, North Carolina, USA) was used to repair and encapsulate the model, which was built as a surface model and exported to Pro/Engineer 5.0 (Parametric Technology Corporation, Needham, Massachusetts, USA) in IGES (Initial Graphics Exchange Specification) format to generate a solid model of each segment. Then, the model was imported into Hypermesh 14.0 (Altair, Troy, Michigan, USA) to obtain a mesh model and to select the material, and the obtained model was uploaded in the ANSYS 13.0 software (ANSYS Company, Canonsburg, Pennsylvania, USA) to facilitate the FE analysis.

The FE model was constructed and consisted of the cortical and cancellous bone, posterior elements, nucleus, annulus ground substance, annulus fiber, anterior longitudinal ligament, posterior longitudinal ligament, ligamentum flavum, transverse ligament, capsular ligament, interspinous ligament, supraspinous ligament, and bone graft. The elastic modulus and Poisson ratio for each element were obtained from a previous report [17]. The material parameters that were most appropriate to define the behavior of the FE model of the nucleus pulposus were modified to simulate a moderate degeneration of the L4-L5 intervertebral disc [18], while the specific values of the material properties used in the model are presented in Table 1. The FE model of the L3-S1 segment was finally developed. Figure 1 shows the anterior, left side, and posterior view of the FE model. The model was composed of a total of 536741 grids and 874956 nodes.

2. Calf Spine Specimen Preparation

Forty fresh calf lumbar spinal segments (L3–L6) were collected from 15-month-old calves with homogeneous weight and spinal condition. All calf spine specimens were acquired following the National Institutes of Health Guidelines for the Use of Laboratory Animals, and all procedures were approved by

the Nanjing Medical University Committee on Animal Care. The structural integrity of all specimens were checked by X-ray, and specimens with fractures, tumors and severe osteoporosis were excluded. All specimens were wrapped in gauze soaked in saline, and sealed with a double-layer plastic bag, and stored at -20°C. The fresh specimens, once stored at -20°C, did not show any alteration in the structure of the bones and ligaments, and their biomechanical properties did not change [19]. Before the test, the specimens were defrosted in an environment at 4°C for 12 hours and the muscle and adipose tissue were removed. The integrity of the bony structure, lumbar intervertebral disc, FJ and ligament tissue should be maintained by paying attention during the handling of the specimen, which was then covered with gauze soaked in saline to keep it moist. Since the calf specimens possessed a long transverse process, all calf specimens were partially cut (retaining approximately 7 cm in length) in order to facilitate the experiment operation. The two ends of the L3 and L6 segments of the specimen were fixed in a special test mold using Kirschner wires, embedded in self-curing denture powder (dental polymethyl methacrylate), and kept horizontal to facilitate the installing of the specimen on the loading device.

3. Insertion point (IP) Determination

According to the actual clinical surgery method, facetectomy was performed by removing the ventral side of the superior FJ up to the dorsal side. Thus, three commonly used clinical needle IPs were selected: (1) The apex of the superior FJ (as the first IP), (2) The midpoint of the ventral side of the superior FJ (as the second IP), (3) The lowest point of the ventral side of the superior FJ (as the third IP). In this experiment, a trephine with a diameter of 7.5 mm commonly used in clinical surgery was used to simulate the UPF. Figure 2 shows the IPs position in the FE model created by the Mimics 15.0 software.

4. Facetectomy Simulation and Grouping

4.1 FE Model

The channel between the IP and the midpoint of the top edge of the lower vertebral body was established by PETD surgery simulated in MIMICS using a lateral posterior approach. A cylinder was used instead of a trephine to simulate the removal of the superior FJ bone using a Boolean subtraction operation. The Model set to 0 (M0) indicated the intact FE model used to compare the other UPF FE models. The Model 1 (M1) was the FE model of UPF performed through the first IP. The Model 2 (M2) was the FE model of UPF performed through the second IP. The Model 3 (M3) was the FE model of UPF performed through the third IP. Figure 3 shows the FE models after UPF.

4.2 Calf Spine Model

Figure 4 shows the percutaneous lumbar facetectomy instrument (Spinendos, Germany) used in the experiment. First, the tip of the duckbill protective sleeve was pushed from the lateral posterior approach through the lower half of the left intervertebral foramen of the specimen to the level of the upper endplate of the L5. The oblique opening of the sleeve faced the back side of the lumbar spine and the sleeve pressed against the IP on the L5 superior FJ. The sleeve formed an angle of 20° with the coronal surface

of the lumbar spine specimen and was parallel to the plane of the intervertebral disc. The intervertebral foramen was formed and enlarged by the matching trephine through the inner cavity of the protective sleeve. The inner diameter of the enlarged protective sleeve was 8.0 mm, and the outer diameter of the trephine was 7.5 mm. Forty fresh calf spine specimens were randomly divided into 4 groups with 10 specimens in each group. The control group was represented by the intact calf spine. The Group A was represented by the calf spine model in which UPF was performed through the first IP. The Group B was represented by the calf spine model in which UPF was performed through the second IP. The Group C was represented by the calf spine model in which UPF was performed through the third IP. Figure 5 shows the calf spine models after UPF.

5. Model Boundaries and Load Conditions

5.1 FE model

After importing the intact model and the 3 UPF models into Ansys 13.0, the human physiologic parameters, boundary conditions, and applied loads were set to each model. All nodes at the bottom of the S1 segment of each model were set as fully constrained and then, a load of 400 N was applied to the upper end of the L3 vertebral body, which is equivalent to the force of the upper human body. A torque load of 10.0 Nm was set in various directions of the coordinate system (X, Y, Z) to simulate different movements [20]. The range of motion (ROM) and the L4/5 intradiscal maximum pressure (IMP) during flexion, extension, left-right lateral bending, and left-right axial rotation were recorded and compared with the ones in the intact model.

5.2 Calf Spine Model

The calf spine specimens were thawed at room temperature for approximately 8 hours before the experiment, and the temperature of the specimens was kept cold before the test by surrounding the specimens with ice cubes to reduce tissue degeneration. A scalpel was used to perform a horizontal incision of 1 cm parallel to the endplate of the vertebral body in the center of the L4/5 intervertebral disc, the needle to test the pressure (approximately 1 mm in diameter) was inserted parallel to the endplate of the vertebral body into the posterior edge of the intervertebral disc, and the Gaeltec pressure sensor (Gaeltec Devices, UK) was connected to measure the IMP. Before the test, the calf spine specimens were fixed on the Intron E10000 tension and torsion biaxial universal material biomechanical testing machine (INSTRON Corporation, USA) using a special fixture for testing calf spine mechanics. An electronic digital level for spine biomechanical test installed above the special fixture was present to measure lumbar spine ROM (Fig. 6). According to the standards of the calf spine specimen test proposed by Wilke et al. [21], the torque was set to 10 N·m and the constant axial pressure was set to 400 N. The specimens were loaded and unloaded twice to remove their viscoelasticity before measuring the ROM of the calf spine flexion, extension, lateral bending, axial rotation and the L4/5 IMP, in order to ensure the accuracy of the data, and the results were recorded on the third round of measurements, so that relatively stable kinematic test data could be obtained. The specimens were continuously sprayed with saline during the entire test to keep them moist and minimize tissue degeneration.

6. Statistical Analysis

Statistical analysis was performed using SPSS (version 22.0; SPSS, USA). The independent-sample *t*-test was used to compare the difference between the intact and facetectomy group, the mean value and standard deviation (SD) were calculated and the measured data were expressed as “x ± s”. All reported p values were two-tailed, and p values less than 0.05 were considered statistically significant.

Results

1. FE models

1.1 Validation of the FE model

In the model developed in this work, a compressive load of 400 N and pure torque of 10.0 Nm were applied to the upper end plate surface of the L3, simulating flexion, extension, and left-right lateral flexion. Then, the ROM of each segment in L3-S1 was measured. Our test data were compared with the data obtained by 3D FE models from a previous research study to evaluate the validity of the model [22]. Our results showed that the L3-S1 lumbar model in the normal physiologic state established in this simulation possessed an appropriate ROM under various conditions of motion, indicating that the model was appropriate (Figure 7).

1.2 L4/5 IMP

The cloud map of the stress distribution of the L4/5 intervertebral disc was generated using the Ansys 13.0 software. The L4/5 IMP increased the least in M2 and increased the most in M3 compared with its value in M0. The L4/5 IMP in M1 significantly increased in flexion (45.2%) and extension (52.5%) compared with its value in M0. The L4/5 IMP in the flexion, extension, left-right lateral flexion, and left-right axial rotation was slightly increased in M2 compared with its value in M0, which was 9.4%, 10.5%, 6.6%, 7.3%, 9.3%, and 9.8% respectively. The L4/5 IMP in the flexion, extension, and left-right axial rotation significantly increased in M3 compared with its value in M0, which was 55.5%, 68.2%, 56.9%, and 54.5%, respectively (P<0.05). The detailed data are listed in Figure 8.

1.3 ROM

The ROM of the L3-S1 FE model was calculated by Ansys 13.0 software. The ROM increased the least in M2 and increased the most in M3 compared with its value in the M0. The ROM in M1 regarding the left axial rotation increased by 35.5% compared with its value in M0. The ROM in the flexion, extension, left-right lateral flexion, and left-right axial rotation was slightly increased in the M2 compared with its value in M0, which was 4.6%, 9.4%, 5.3%, 4.8%, 8.5%, and 9.2% respectively, The ROM of the lumbar spine in the right lateral flexion and left-right axial rotation was significantly increased in the M3 compared with its value in M0, which was 37.1%, 43.7%, and 40.4%, respectively (P<0.05). The detailed data are listed in Figure 9.

2. Calf Spine Models

2.1 L4/5 IMP

The data of the pressure sensor in the L4/5 intervertebral disc of the calf spine specimen were recorded and analyzed. The L4/5 IMP significantly increased under extension in the group A compared with the control group (P<0.05). The L4/5 IMP slightly increased in the group B compared with its value in the control group during extension and left-right axial rotation, but the difference was not statistically significant. The difference in flexion and left-right lateral flexion was also not statistically significant compared with the control group. The L4/5 IMP significantly increased in the group C under extension and left-right axial rotation compared with its value in the control group (P<0.05). The detailed data are listed in Table 2.

2.2 ROM

The ROM of the calf spine specimens was obtained by recording the electronic digital level on the upper end of the specimen fixture (Table 3). No significant difference in ROM was found under the six motions of flexion and extension, left-right lateral flexion and left-right axial rotation in group A and group B compared with the control group. However, the ROM was significantly increased under left-right axial rotation in the group C compared with its value in the control group (P < 0.05).

Discussion

Many studies reported that the deterioration of the biomechanical function is the most crucial reason for postoperative complications such as lumbar instability [23–26], which in turn causes chronic low back pain in the patients [27–29]. At present, lumbar instability is diagnosed by the relative displacement or angle of the vertebral body in the flexion and extension positions. Hasegawa K. et.al also believe that the increase in the FJ space is the strongest predictor of lumbar instability [30]. Therefore, the integrity and health of the FJs are essential in the stability of the lumbar spine. FE analysis is considered as an important method in biomechanics research, since it effectively replaces the human body research and provides bio-realistic results in terms of trend analyses. According to different studies, the properties of materials can be changed by FE analysis, which can also generate and manipulate geometric shapes as needed [31–33]. The best choice for testing the biomechanics of lumbar spine is the use of specimens from a fresh human cadaver. However, it is difficult to obtain a sufficient number of cadavers of the same age and gender. Therefore, animal specimens are the best choice for biomechanical experiments rather than specimens from human cadavers, and they can be obtained from several animals including dogs, pigs, calves, and sheep. Among them, calf vertebral bodies are similar in size to the human ones and have a wide variety of sources. Therefore, the experiments in this work were performed using 40 calf spine specimens to perform UPF.

During the PETD surgery, an insertion operation is performed under local anesthesia in the posterior aspect of the vertebral body to allow the direct entry into the spinal canal to perform the discectomy. The

surgery is performed far from the outlet and dorsal root ganglia, avoiding as much as possible the muscles and ligaments adjacent to the vertebral body, but a partial destruction of the FJ is inevitable. Some biomechanical studies showed that the destruction of FJs increases the risk of spinal instability and spinal degeneration [34–36]. However, recent advances in FE research on facetectomy have been made. In 2014, Erbulut [37] performed an FE analysis and found that the FE model of the lumbar spine is severely affected in extension and axial rotation after the complete removal of one FJ side. Thus, lumbar fusion or pedicle screw fixation is required after the removal of the bilateral FJs of the lumbar spine. However, in 2017, Zeng et al. [7] simulated the resection of the 50% of one FJ side on a lumbar FE model and they realized that the intradiscal pressure and intervertebral ROM were not significantly different from their value in the intact model. Thus, these patients do not need lumbar fusion or lumbar fixation. On the other hand, in 2019, Li et al. [38] simulated the graded resection of the lumbar FJs through FE analysis and discovered that the removal of the 50% of the unilateral lumbar FJ increased the risk of biomechanical degeneration of the lumbar spine and the occurrence of failed back surgery syndrome. In 2020, S. Ahuja et al. [16] performed an FE analysis and discovered that the lumbar spine ROM, the pressure in the FJs and the pressure in the intervertebral disc significantly increase when more than 30% of an unilateral facet joint is removed. The conclusions of the above studies on the biomechanics of facetectomy are different, because none of these studies established a unified standard in the resection of the lumbar FJs. The experiments performed in previous works were mostly resection of the superior FJ from the dorsal side to the ventral side, which is not in agreement with what is performed in clinical practice, and the cutting method was a longitudinal cut of artificial division [16, 37–41]. Indeed, a trephine is used in clinical practice to perform a cut from the ventral side of the superior FJ to the dorsal side, and from the head to the tail end [42–44]. The resected superior FJ is left with an arc-shaped gap. Therefore, the previous studies are not applicable in clinical surgery, thus having less significance.

The three IPs selected in our experiments were needle IPs currently used in clinical surgery, with the first IP (the apex of the superior FJ) as the most commonly used IP. The percutaneous endoscopic discectomy was invented in 1993 by the German spine surgeon Hoogland Thomas [45] who chose the apex of the superior FJ as the needle IP [46, 47]. Therefore, this IP was selected also in this work as one of the IPs to perform the experiments. In our experiment, the height of the L5 superior FJ of the lumbar FE model was 13.4 mm, the average height of the L5 superior FJ of the calf spine models was greater than 13 mm, and the radius of the trephine was 3.75 mm, thus, the height of the superior FJ was sufficient to divide the three IPs, all placed at the edge of the superior FJ. Facetectomy performed through the ventral edge of the superior FJ can maximize the expansion of the intervertebral foramen. In addition, the test data on these three IPs could be compared with each other to evaluate the impact of facetectomy of the different FJ portions on the biomechanics of the lumbar spine.

The bilateral FJs and the intervertebral disc form a spine unit that shares the pressure of the trunk on the vertebral body [48–50]. Since the top of the superior FJ is triangular, a stress concentration may easily occur at the tip of the superior FJ under physiological conditions, meaning that the stress sustained in this point is relatively large. The facetectomy performed through the first IP resulted in a destruction of the integrity of the superior FJ, leading to stress redistribution, and the larger stress sustained by the apex

of the superior FJ was distributed to the adjacent intervertebral disc and the contralateral FJ. The FE analysis revealed that the ROM of the lumbar spine in M1 was increased by 35.5% compared with its value in M0 in the left axial rotation, and the L4/5 IMP during flexion and extension was increased by 45.2% and 52.5% respectively, compared with their values in M0. However, the *in vitro* biomechanics test revealed no significant difference in the ROM of the lumbar spine after facetectomy of the calf spine models between the group A and B compared with the control group. This might be related to the protection of the joint capsule of the FJs. Indeed, some studies showed that the joint capsule of the FJs not only protects and nourishes the FJs, but also shares the physiological load, thus limiting the excessive movement of the lumbar spine [10, 51, 52]. The second IP was located on the outer edge of the intervertebral foramen. The FE analysis revealed that the volume of the superior FJ removed through the second IP was the smallest compared with the volume removed through the other IPs, and the damage on the joint capsule of the FJ was also the smallest. M2 did not show any significant increase in the ROM and L4/5 IMP of the lumbar spine during flexion, extension, left-right flexion and left-right axial rotation compared with their values in M0. In the *in vitro* biomechanics test, no statistically significant difference was found in the L4/5 IMP and ROM of the lumbar spine in the group B compared with the control group. The third IP was performed in the thickest part of the superior FJ, where the stress was the largest. FE analysis revealed that the L4/5 IMP and the ROM of the lumbar spine of the M3 were significantly increased compared with their values in M0. The *in vitro* biomechanics test revealed a statistically significant difference in the L4/5 IMP and ROM of the lumbar spine in the C group compared with the control group. Therefore, the results of the FE analysis were consistent with the results of the *in vitro* biomechanics test.

This work has a limitation. No specimens from cadavers were used to perform the *in vitro* biomechanical studies due to the reasons explained above in articles already published, thus, calf spine specimens were preferred since calf vertebral bodies are similar in size to the human ones, and because calf spine specimens represent the best replacement for cadaver spine specimens to perform biomechanical research. However, in the present experiments the FJs of the calf spine specimens possessed thicker joint capsules and greater bone density, which increased the difficulty in the removal of the excess muscle and soft tissues from the specimens. The outer diameter of the trephine used in the experiment was 7.5 mm, therefore, the biomechanical effect of other size trephine or tools used for facetectomy on the lumbar spine needs further study and additional clinical research.

Conclusions

In conclusion, although the first IP is the most commonly used IP in the PTED surgery, our results showed that it was not the most appropriate IP in the analysis of FE biomechanics and *in vitro* biomechanical experiment. UPF performed through the midpoint of the ventral side of the superior FJ resulted in a minimal impact on the biomechanics of the lumbar spine, suggesting that it might be the most appropriate IP for UPF. Our conclusion allows the refinement of the current guidelines in performing percutaneous endoscopy, providing a theoretical basis for clinicians in the choice of the most appropriate IP to perform UPF.

Abbreviation

1. insertion point (IP)
2. insertion points (IPs)
3. percutaneous endoscopic transforaminal discectomy (PETD)
4. unilateral partial facetectomy (UPF)
5. facet joint (FJ)
6. facet joints (FJs)
7. range of motion (ROM)
8. transforaminal endoscopic spine system (TESSYS)
9. lumbar disc herniation (LDH)

Declarations

Funding

This study was supported by “General project of Jiangsu Provincial Department of health(H2019025)”, “The Project of invigorating Health Care through Science, Technology and Education (Jiangsu Provincial Medical Youth Talent), Changzhou High-level Medical Talents Training Project (2016CZBJ029)", “Six Talent Peaks Project, Jiangsu Provincial Finance Department (WSW-186)” , “Jiangsu Provincial Social Development Project (BE2020650)” and “Changzhou International Science and Technology Cooperation Project (CZ20200037)”.

Conflicts of interest/Competing interests

No conflict of interest exits in the submission of this manuscript, and manuscript is appproved by all authors for publication.

Ethics approval

This study was approved by the ethics committee of The Affiliated Changzhou No.2 People’s Hospital of Nanjing Medical University. The number is 2020022830121.

Consent to participate

All authors declare that they have participated in the writing of the article and the operation of the experiment.

Consent for publication

All authors agree to publish this article.

Availability of data and material

The datasets generated and analyzed during the present study are available from the corresponding author on reasonable request.

Code availability

Not applicable

Authors' contributions

LR and NM performed most of the investigation, data analysis and wrote the manuscript; LT contributed to interpretation of the data and analyses. All of the authors have read and approved the manuscript.

References

1. SS, H., R, P., S, W. & R, B. Balance Control in Patients with Subacute Non-Specific Low Back Pain, with and without Lumbar Instability: A Cross-Sectional Study. *Journal of pain research* 13, 795-803, doi:10.2147/jpr.s232080 (2020).
2. C, S., WJ, T., HX, L. & PG, G. Outcomes of multisegmental transforaminal enlarged decompression plus posterior pedicle screw fixation for multilevel lumbar spinal canal stenosis associated with lumbar instability. *International journal of surgery (London, England)* 50, 72-78, doi:10.1016/j.ijsu.2017.12.031 (2018).
3. T, H., K, v. d. B.-D., M, S. & B, M. Endoscopic transforaminal discectomy for recurrent lumbar disc herniation: a prospective, cohort evaluation of 262 consecutive cases. *Spine* 33, 973-978, doi:10.1097/BRS.0b013e31816c8ade (2008).
4. G, G. *et al.* Percutaneous Transforaminal Endoscopic Discectomy for Adjacent Segment Disease After Lumbar Fusion in Elderly Patients Over 65 Years Old. *World neurosurgery* 112, e830-e836, doi:10.1016/j.wneu.2018.01.170 (2018).
5. X, L. *et al.* The Effects of Orientation of Lumbar Facet Joints on the Facet Joint Contact Forces: An In Vitro Biomechanical Study. *Spine* 43, E216-E220, doi:10.1097/brs.0000000000002290 (2018).
6. Kiapour, A., Ambati, D., Hoy, R. W. & Goel, V. K. Effect of graded facetectomy on biomechanics of dynesys dynamic stabilization system. *Spine* 37, E581–E589, doi:10.1097/BRS.0b013e3182463775 (2012).
7. Zeng, Z.-l., Zhu, R. & Wu, Y.-C. Effect of Graded Facetectomy on Lumbar Biomechanics. *J Healthc Eng* 2017, 7981513, doi:10.1155/2017/7981513 (2017).
8. Li, X. *et al.* Biomechanical Model Study of the Effect of Partial Facetectomy on Lumbar Stability Under Percutaneous Endoscopy. *World neurosurgery* 139, e255-e264, doi:10.1016/j.wneu.2020.03.190 (2020).

9. TR, H. *et al.* The role of the lumbar facet joints in spinal stability. Identification of alternative paths of loading. *Spine* 19, 2667-2670 discussion 2671 (1994).
10. EA, B., VH, B. & AM, E. The role of the facet capsular ligament in providing spinal stability. *Computer methods in biomechanics and biomedical engineering* 21, 712-721, doi:10.1080/10255842.2018.1514392 (2018).
11. WK, C. *et al.* Predictors of Pain Recurrence After Lumbar Facet Joint Injections. *Frontiers in neuroscience* 13, 958, doi:10.3389/fnins.2019.00958 (2019).
12. H, S., F, G., A, R., T, Z. & HJ, W. Effect of multilevel lumbar disc arthroplasty on spine kinematics and facet joint loads in flexion and extension: a finite element analysis. *European spine journal : official publication of the European Spine Society, the European Spinal Deformity Society, and the European Section of the Cervical Spine Research Society*, S663-674, doi:10.1007/s00586-010-1382-1 (2012).
13. TJ, Y., SW, T., F, L. M. & P, P. Comparison of adjacent segment disease after minimally invasive or open transforaminal lumbar interbody fusion. *Journal of clinical neuroscience : official journal of the Neurosurgical Society of Australasia* 21, 1796-1801, doi:10.1016/j.jocn.2014.03.010 (2014).
14. GR, E. *et al.* Degeneration and Instability and the Relation to Patients' Function Late After Lumbar Disc Surgery: Data from a 12-Year Follow-Up. *American journal of physical medicine & rehabilitation* 95, 871-879, doi:10.1097/phm.0000000000000522 (2016).
15. KE, R. *et al.* Adjacent segment disease in the lumbar spine following different treatment interventions. *The spine journal : official journal of the North American Spine Society* 13, 1339-1349, doi:10.1016/j.spinee.2013.03.020 (2013).
16. Ahuja, S. *et al.* Lumbar stability following graded unilateral and bilateral facetectomy: A finite element model study. *Clin Biomech (Bristol, Avon)* 75, 105011, doi:10.1016/j.clinbiomech.2020.105011 (2020).
17. CS, C., CK, C., CL, L. & WH, L. Stress analysis of the disc adjacent to interbody fusion in lumbar spine. *Medical engineering & physics* 23, 483-491, doi:10.1016/s1350-4533(01)00076-5 (2001).
18. LM, R., RN, N. & GB, A. Influence of single-level lumbar degenerative disc disease on the behavior of the adjacent segments--a finite element model study. *Journal of biomechanics* 42, 341-348, doi:10.1016/j.jbiomech.2008.11.024 (2009).
19. Park, S., Lim, T. & Park, J. A biomechanical study of the instrumented and adjacent lumbar levels after In-Space interspinous spacer insertion. *Journal of neurosurgery. Spine* 12, 560-569, doi:10.3171/2009.11.spine08668 (2010).
20. Coombs, D., Rullkoetter, P. & Laz, P. Efficient probabilistic finite element analysis of a lumbar motion segment. *Journal of biomechanics* 61, 65-74, doi:10.1016/j.jbiomech.2017.07.002 (2017).
21. HJ, W., B, M., S, M. & N, G. Development of a scoliotic spine model for biomechanical in vitro studies. *Clinical biomechanics (Bristol, Avon)* 30, 182-187, doi:10.1016/j.clinbiomech.2014.12.002 (2015).
22. Yamamoto, I., Panjabi, M., Crisco, T. & Oxland, T. Three-dimensional movements of the whole lumbar spine and lumbosacral joint. *Spine* 14, 1256-1260, doi:10.1097/00007632-198911000-00020 (1989).

23. Adams, M., Freeman, B., Morrison, H., Nelson, I. & Dolan, P. Mechanical initiation of intervertebral disc degeneration. *Spine* 25, 1625-1636, doi:10.1097/00007632-200007010-00005 (2000).
24. Más, Y. *et al.* Finite element simulation and clinical follow-up of lumbar spine biomechanics with dynamic fixations. *PloS one* 12, e0188328, doi:10.1371/journal.pone.0188328 (2017).
25. Hsieh, Y. *et al.* Removal of fixation construct could mitigate adjacent segment stress after lumbosacral fusion: A finite element analysis. *Clinical biomechanics (Bristol, Avon)* 43, 115-120, doi:10.1016/j.clinbiomech.2017.02.011 (2017).
26. Tang, S. & Rebholz, B. Does lumbar microdiscectomy affect adjacent segmental disc degeneration? A finite element study. *The Journal of surgical research* 182, 62-67, doi:10.1016/j.jss.2012.09.012 (2013).
27. Hlaing, S., Puntumetakul, R., Wanpen, S. & Boucaut, R. Balance Control in Patients with Subacute Non-Specific Low Back Pain, with and without Lumbar Instability: A Cross-Sectional Study. *Journal of pain research* 13, 795-803, doi:10.2147/jpr.s232080 (2020).
28. Denteneer, L., Stassijns, G., De Hertogh, W., Truijen, S. & Van Daele, U. Inter- and Intrarater Reliability of Clinical Tests Associated With Functional Lumbar Segmental Instability and Motor Control Impairment in Patients With Low Back Pain: A Systematic Review. *Archives of physical medicine and rehabilitation* 98, 151-164.e156, doi:10.1016/j.apmr.2016.07.020 (2017).
29. Ferrari, S., Manni, T., Bonetti, F., Villafañe, J. & Vanti, C. A literature review of clinical tests for lumbar instability in low back pain: validity and applicability in clinical practice. *Chiropractic & manual therapies* 23, 14, doi:10.1186/s12998-015-0058-7 (2015).
30. K, H., H, S., K, K., K, S. & T, H. What are the reliable radiological indicators of lumbar segmental instability? *The Journal of bone and joint surgery. British volume* 93, 650-657, doi:10.1302/0301-620x.93b5.25520 (2011).
31. Tropiano, P. *et al.* Using a finite element model to evaluate human injuries application to the HUMOS model in whiplash situation. *Spine* 29, 1709-1716, doi:10.1097/01.brs.0000135840.92373.5c (2004).
32. Hussain, M., Nassr, A., Natarajan, R., An, H. & Andersson, G. Biomechanical effects of anterior, posterior, and combined anterior-posterior instrumentation techniques on the stability of a multilevel cervical corpectomy construct: a finite element model analysis. *The spine journal : official journal of the North American Spine Society* 11, 324-330, doi:10.1016/j.spinee.2011.02.008 (2011).
33. Johnson, W. & Fischer, D. Skeletal stabilization with a multiplane external fixation device. Biomechanical evaluation and finite element model. *Clinical orthopaedics and related research*, 34-43 (1983).
34. Okuda, S. *et al.* Surgical complications of posterior lumbar interbody fusion with total facetectomy in 251 patients. *Journal of neurosurgery. Spine* 4, 304-309, doi:10.3171/spi.2006.4.4.304 (2006).
35. Sairyo, K., Chikawa, T. & Nagamachi, A. State-of-the-art transforaminal percutaneous endoscopic lumbar surgery under local anesthesia: Discectomy, foraminoplasty, and ventral facetectomy. *Journal of orthopaedic science : official journal of the Japanese Orthopaedic Association* 23, 229-236, doi:10.1016/j.jos.2017.10.015 (2018).

36. Phillips, F. *et al.* Effect of the Total Facet Arthroplasty System after complete laminectomy-facetectomy on the biomechanics of implanted and adjacent segments. *The spine journal : official journal of the North American Spine Society* 9, 96-102, doi:10.1016/j.spinee.2008.01.010 (2009).
37. Erbulut, D. & Erbulut, D. Biomechanical effect of graded facetectomy on asymmetrical finite element lumbar spine. *Turkish Neurosurgery*, doi:10.5137/1019-5149.jtn.11984-14.2 (2014).
38. Qian Jun, Yu Shuisheng, Liu Jianjun, Chen Li & Juehua, J. Biomechanics changes of lumbar spine caused by foraminotomy via percutaneous transforaminal endoscopic lumbar discectomy. *National Medical Journal of China* 98, 1013-1018, doi:10.3760/cma.j.issn.0376-2491.2018.13.012 (2018).
39. Kiapour, A., Ambati, D., Hoy, R. & Goel, V. Effect of graded facetectomy on biomechanics of Dynesys dynamic stabilization system. *Spine* 37, E581-589, doi:10.1097/BRS.0b013e3182463775 (2012).
40. Lee, K., Teo, E., Qiu, T. & Yang, K. Effect of facetectomy on lumbar spinal stability under sagittal plane loadings. *Spine* 29, 1624-1631, doi:10.1097/01.brs.0000132650.24437.15 (2004).
41. J, L., X, Z., W, X., Z, X. & L, X. Reducing the extent of facetectomy may decrease morbidity in failed back surgery syndrome. *BMC musculoskeletal disorders* 20, 369, doi:10.1186/s12891-019-2751-5 (2019).
42. Xie, P. *et al.* Percutaneous transforaminal full endoscopic decompression for the treatment of lumbar spinal stenosis. *BMC musculoskeletal disorders* 21, 546, doi:10.1186/s12891-020-03566-x (2020).
43. Wang, Y. *et al.* Percutaneous Transforaminal Endoscopic Discectomy and Fenestration Discectomy to Treat Posterior Ring Apophyseal Fractures: A Retrospective Cohort Study. *Orthopaedic surgery*, doi:10.1111/os.12698 (2020).
44. Chen, Z. *et al.* Percutaneous transforaminal endoscopic discectomy compared with microendoscopic discectomy for lumbar disc herniation: 1-year results of an ongoing randomized controlled trial. *Journal of neurosurgery. Spine* 28, 300-310, doi:10.3171/2017.7.spine161434 (2018).
45. Hoogland, T. Percutaneous endoscopic discectomy. *Journal of neurosurgery* 79, 967-968 (1993).
46. Schubert, M. & Hoogland, T. Endoscopic transforaminal nucleotomy with foraminoplasty for lumbar disk herniation. *Operative Orthopadie und Traumatologie* 17, 641-661, doi:10.1007/s00064-005-1156-9 (2005).
47. Hoogland, T., van den Brekel-Dijkstra, K., Schubert, M. & Miklitz, B. Endoscopic transforaminal discectomy for recurrent lumbar disc herniation: a prospective, cohort evaluation of 262 consecutive cases. *Spine* 33, 973-978, doi:10.1097/BRS.0b013e31816c8ade (2008).
48. Abbas, J. *et al.* In the quest for degenerative lumbar spinal stenosis etiology: the Schmorl's nodes model. *BMC musculoskeletal disorders* 18, 164, doi:10.1186/s12891-017-1512-6 (2017).
49. Li, Z. *et al.* Miniopen Transforaminal Lumbar Interbody Fusion with Unilateral Fixation: A Comparison between Ipsilateral and Contralateral Reherniation. *BioMed research international* 2016, 7261027, doi:10.1155/2016/7261027 (2016).
50. Szkoda-Poliszuk, K., Żak, M. & Pezowicz, C. Finite element analysis of the influence of three-joint spinal complex on the change of the intervertebral disc bulge and height. *International journal for numerical methods in biomedical engineering* 34, e3107, doi:10.1002/cnm.3107 (2018).

51. Widmer, J. *et al.* Biomechanical contribution of spinal structures to stability of the lumbar spine-novel biomechanical insights. *The spine journal : official journal of the North American Spine Society*, doi:10.1016/j.spinee.2020.05.541 (2020).
52. Zehr, J., Barrett, J., Fewster, K., Laing, A. & Callaghan, J. Strain of the facet joint capsule during rotation and translation range-of-motion tests: an in vitro porcine model as a human surrogate. *The spine journal : official journal of the North American Spine Society* 20, 475-487, doi:10.1016/j.spinee.2019.09.022 (2020).

Tables

Table 1. The Material Properties Specified in the Finite Element Models

Number	Material	Young's modulus（MPa)	Poisson's ratio	Cross-section（mm2）
1	cortical bone	12000.00	0.30	—
2	cancellous bone	100.00	0.20	—
3	posterior elements	3500.00	0.25	—
4	annulus fiber	175.00	—	0.76
5	annulus ground substance	4.20	0.45	—
6	nucleus	1.00	0.50	—
7	moderate degeneration of nucleus	1.66	0.40	—
8	ALL（anterior longitudinal ligament）	7.8(ε<12%), 20(ε>12%)	—	63.70
9	PLL（posterior longitudinal ligament）	10(ε<11%), 20(ε>11%)	—	20.00
10	LF(ligamentum flavum)	15(ε<6.2%), 19.5(ε>6.2%)	—	40.00
11	TL(transverse ligament)	10(ε<18%), 58.7(ε>18%)	—	1.80
12	CL(capsular ligament)	7.5(ε<25%), 32.9(ε>25%)	—	30.00
13	IL(interspinous ligament)	10(ε<14%), 11.6(ε>14%)	—	40.00
14	SL(supraspinous ligament)	8(ε<20%), 15(ε>20%)	—	30.00
15	Bone graft	3500	0.25	—

(ε: strain)

TABLE 2. The L4/5 Intradiscal Maximum Pressure of Calf Spine Specimens After Facetectomy（KPa）

Grouping	Control	A	B	C	*P* value
Flexion	572.48±23.38	694.91±29.65	654.64±15.99	729.48±24.22	*P*<0.001
Extension	627.53±41.22	941.51±39.62[a]	714.05±41.35	1000.23±52.32[a]	*P*<0.001
Left lateral flexion	556.37±43.42	682.89±51.74	638.08±33.68	715.79±46.29	*P*<0.001
Right lateral flexion	578.47±52.12	705.20±55.48	664.88±43.15	738.40±46.53	*P*<0.001
Left rotation	685.28±37.42	794.08±48.26	742.27±33.82	1123.47±33.58[a]	*P*<0.001
Right rotation	663.78±46.96	786.45±45.92	725.11±47.15	1047.60±51.62[a]	*P*<0.001

Note: Compared to the control group，[a] *P*<0.05

TABLE 3. The Range of Motion of Calf Spine Specimens After Facetectomy（°）

Grouping	Control	A	B	C	*P* value
Flexion	10.23±2.09	11.44±3.29	11.55±2.12	12.68±3.11	P<0.001
Extension	7.20±1.77	7.85±1.64	7.65±0.84	8.15±1.14	P<0.001
Left lateral flexion	8.33±1.27	8.95±1.19	8.90±1.11	10.45±1.53	P<0.001
Right lateral flexion	8.85±1.25	9.47±1.34	8.95±1.18	10.15±1.20	P<0.001
Left rotation	4.80±0.75	5.35±0.68	5.20±0.76	9.23±1.50[a]	P<0.001
Right rotation	5.85±0.84	6.35±0.67	6.55±0.75	10.15±1.44[a]	P<0.001

Note: Compared to the control group[a] *P*<0.05

Figures

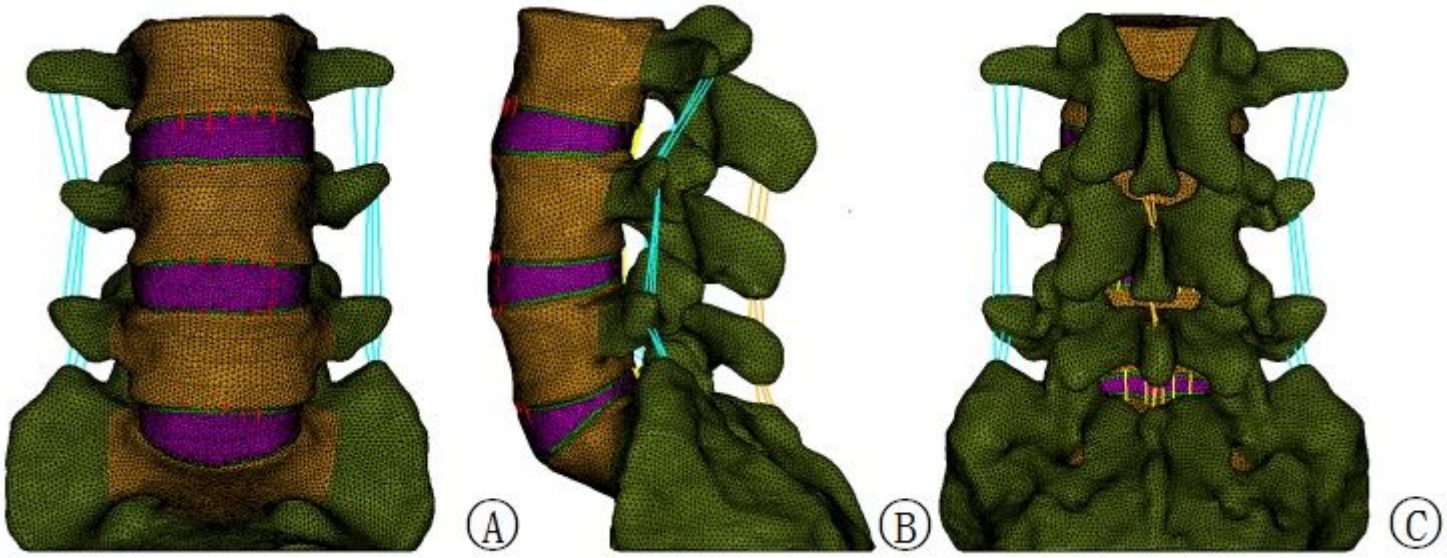

Figure 1

A: The anterior of the finite element model. B: The left side of the finite element model. C: The posterior of the finite element model.

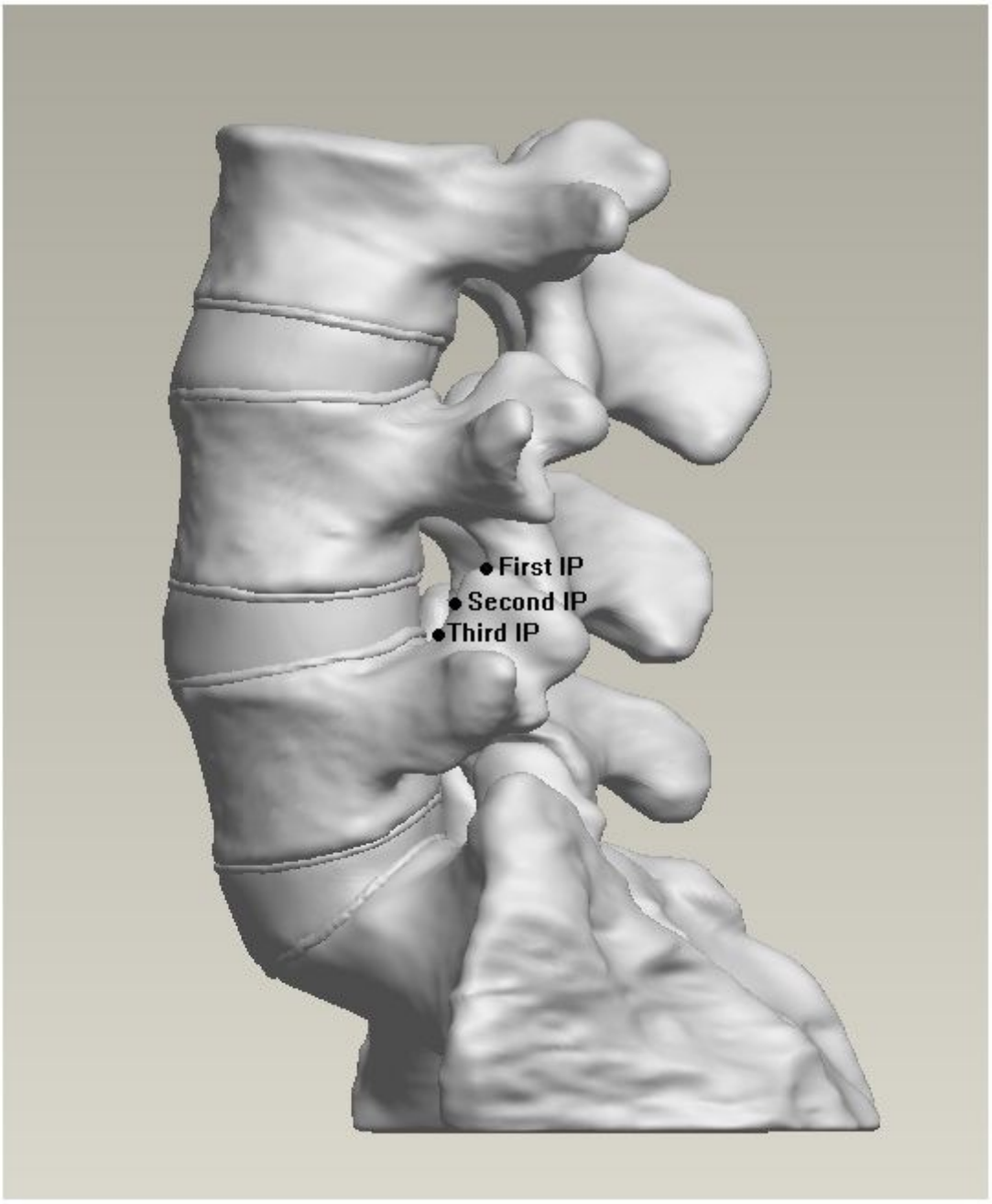

Figure 2

The 3 insertion points of the facet joint of L5 in the finite element model.

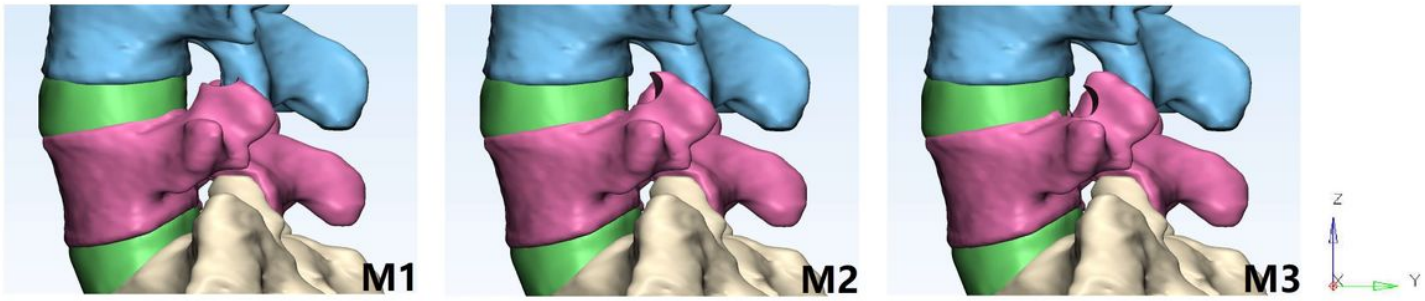

Figure 3

The schematic diagram of L5 left superior facet joint resection in the finite element models.

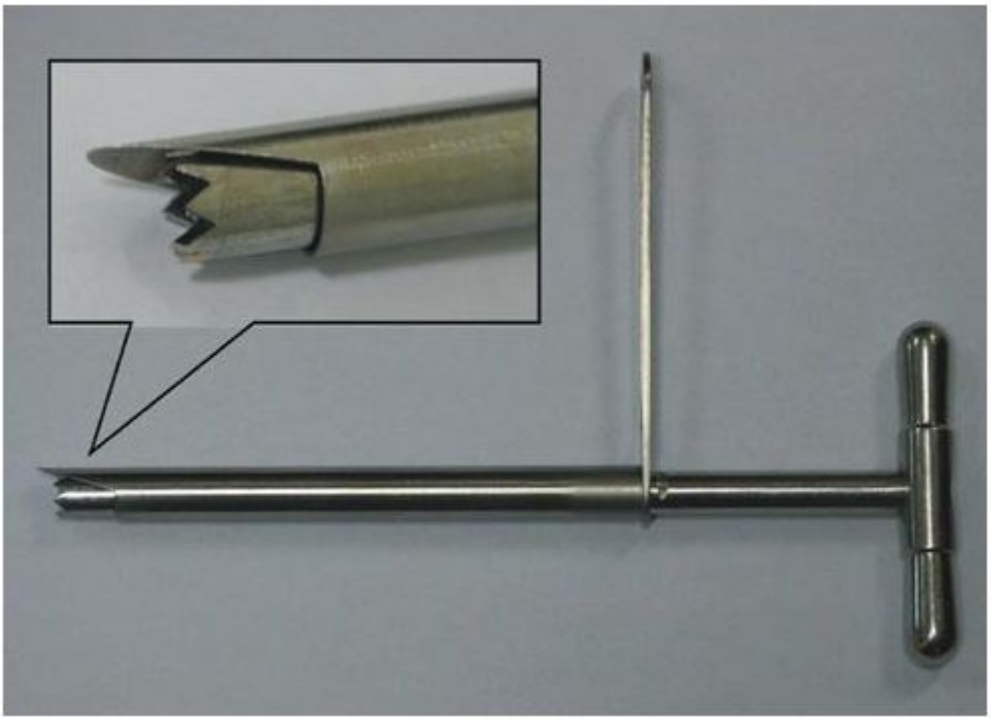

Figure 4

The trephine (Spinendos, Germany) used in the biomechanical experiment of calf spine specimens.

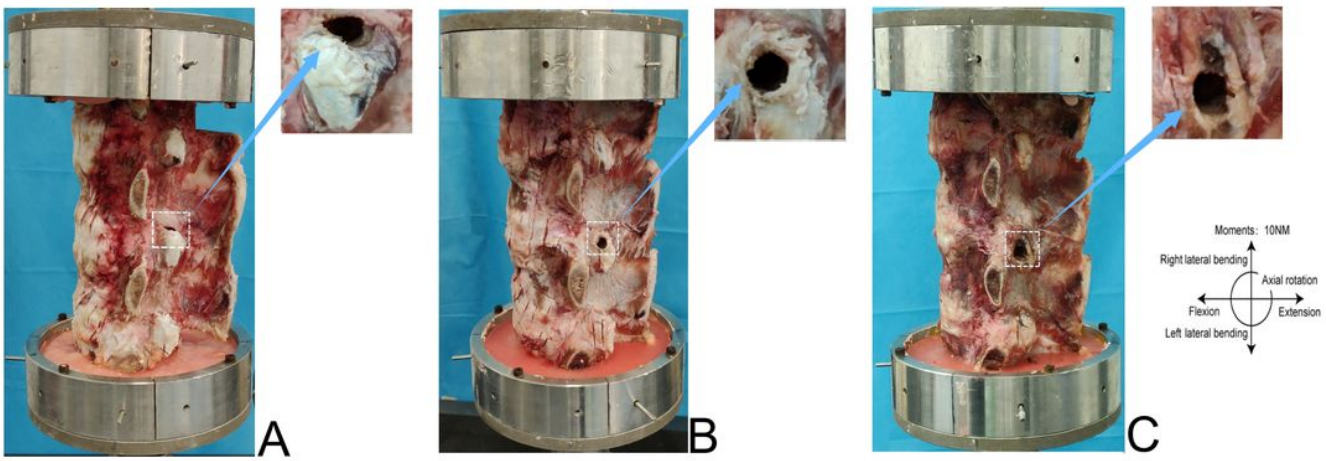

Figure 5

The schematic diagram of L5 left superior facet joint resection in the calf spine specimens: A: Group A. B: Group B. C: Group C.

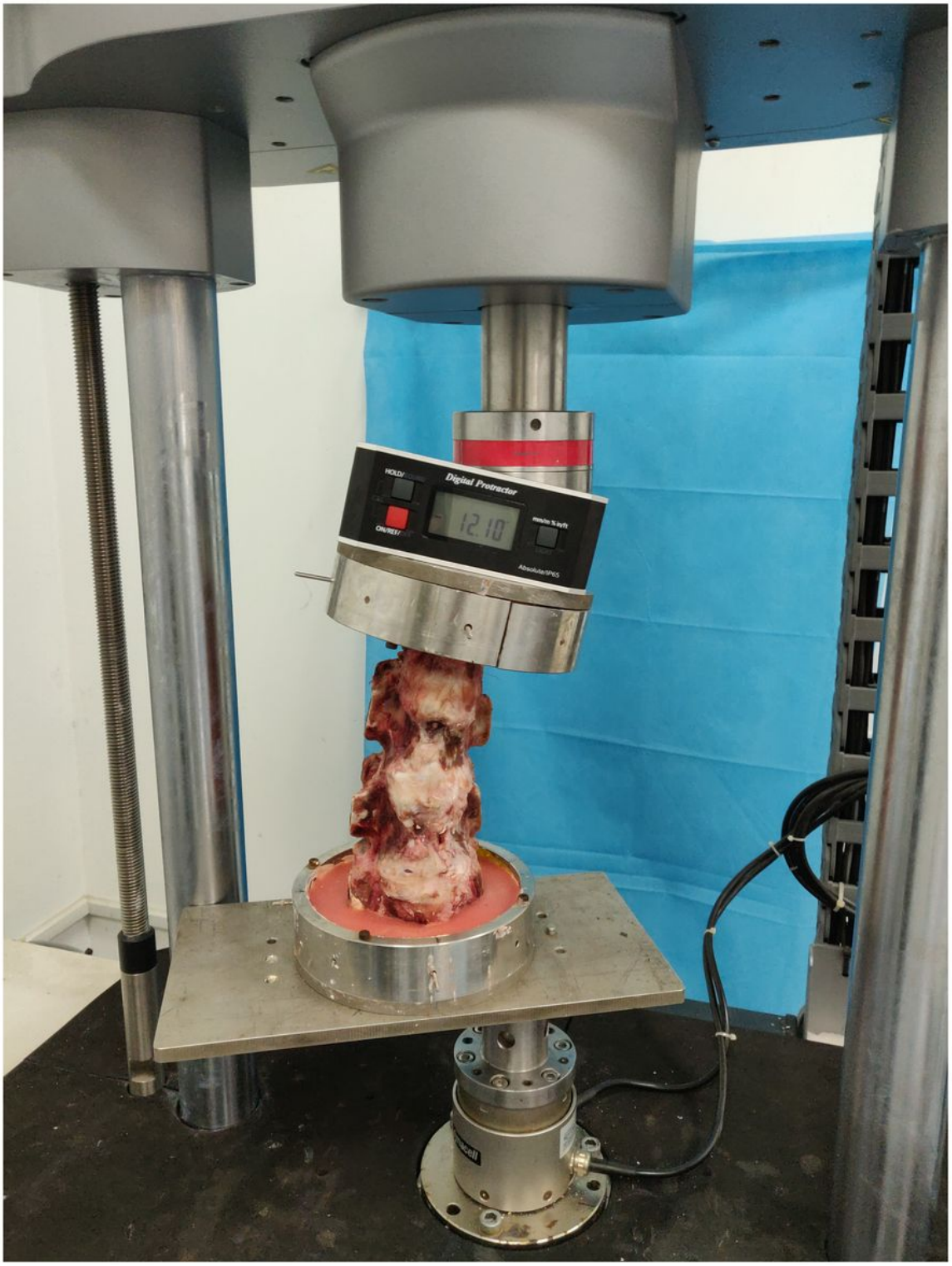

Figure 6

The Intron E10000 tension and torsion biaxial universal material biomechanical testing machine (INSTRON Corporation, USA) and electronic digital level for calf spine specimens biomechanical test.

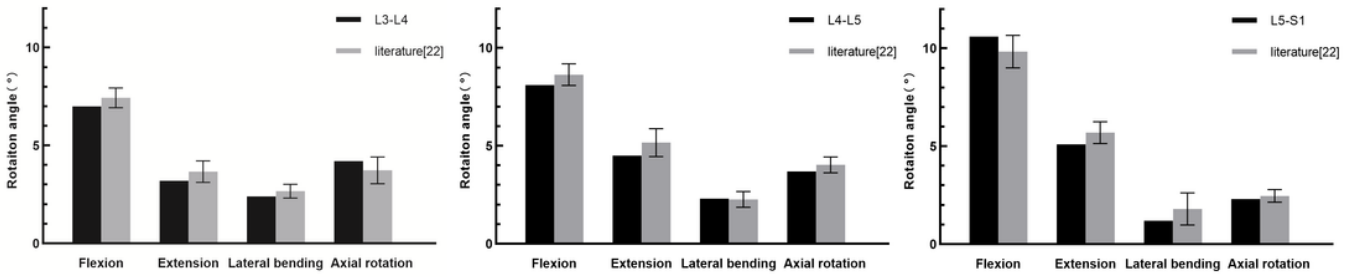

Figure 7

Comparison of range of motion between the segments of the established L3-S1 model and previous research study.

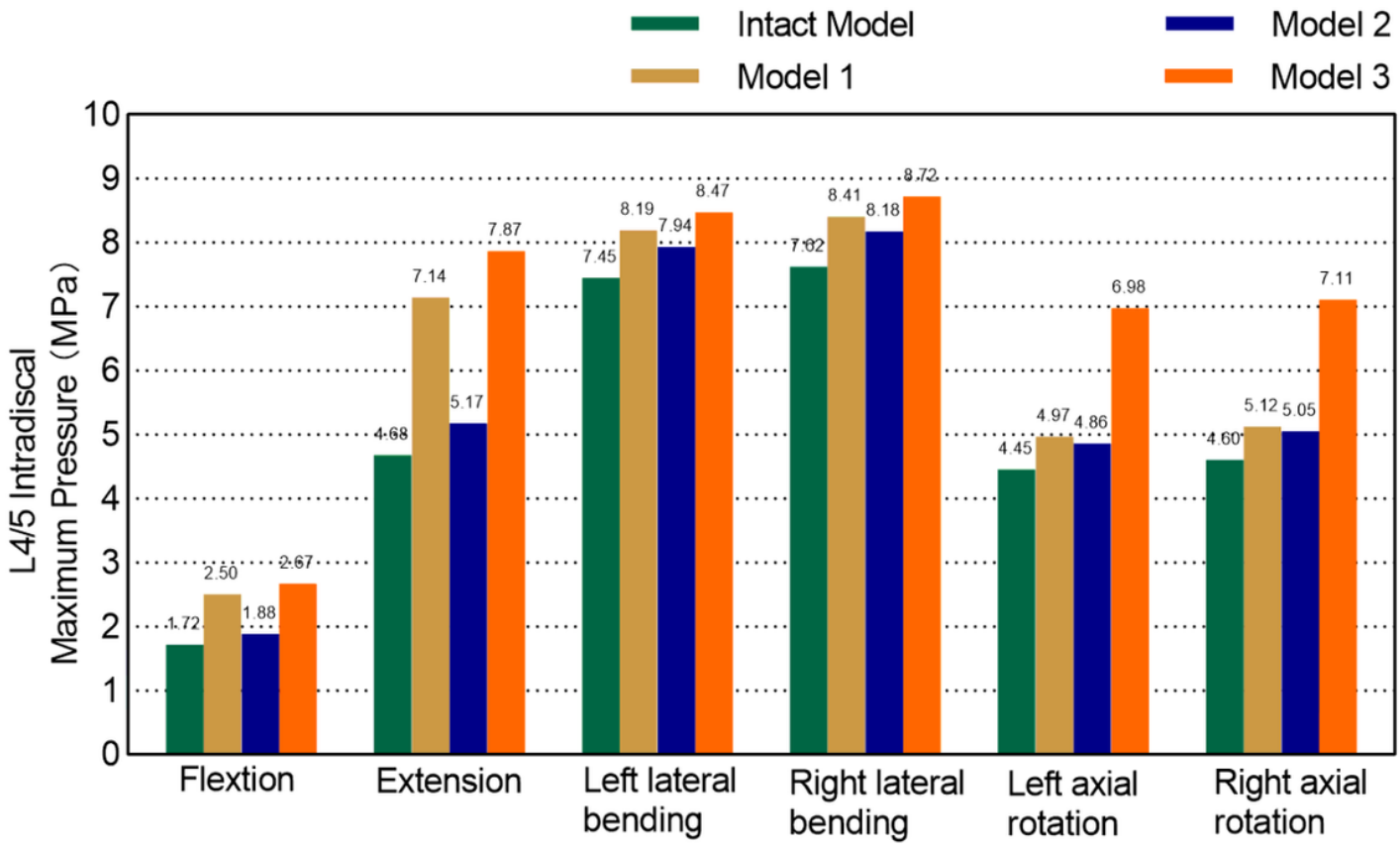

Figure 8

Changes of the L4/5 intradiscal maximum pressure after facetectomy (Mpa).

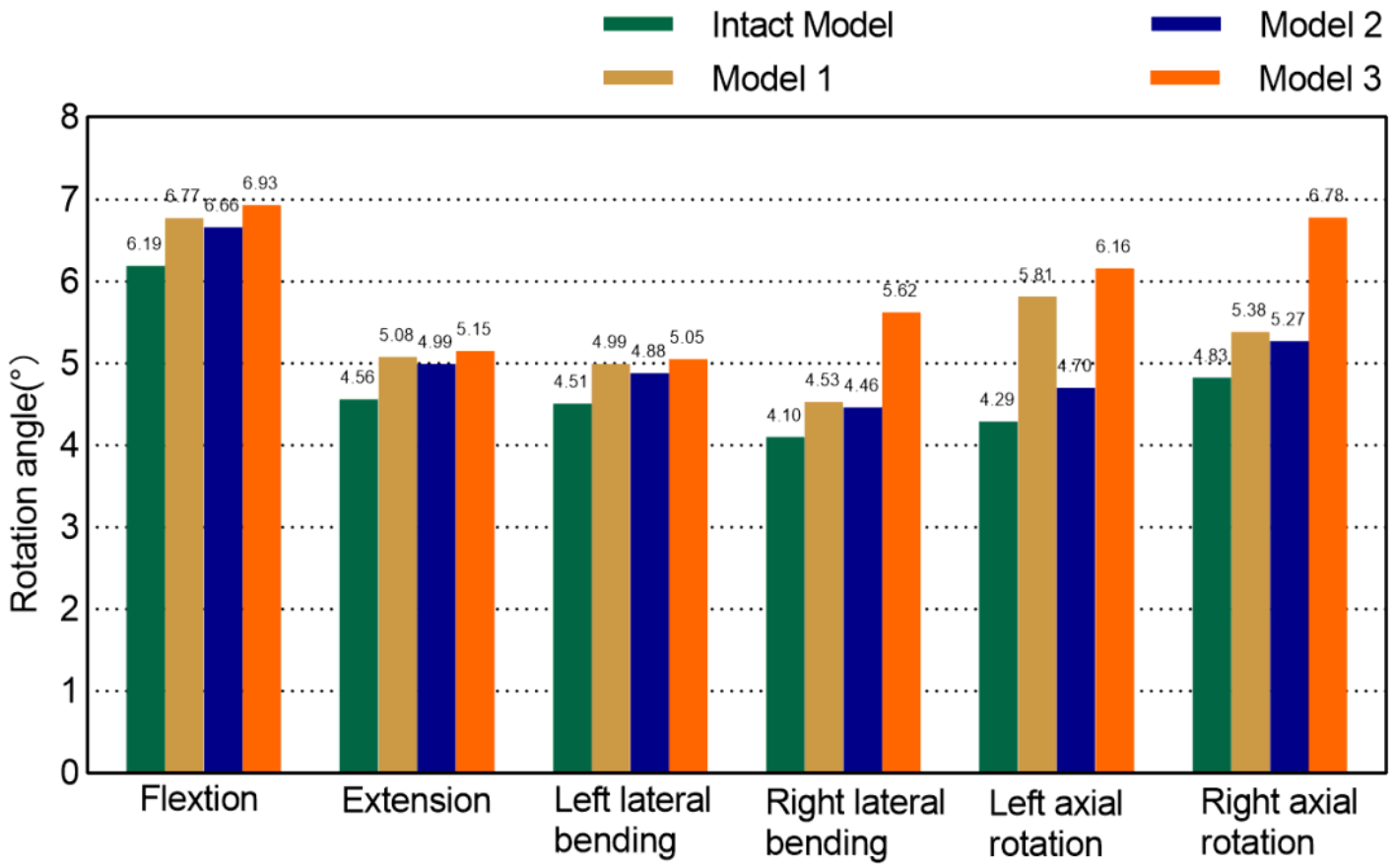

Figure 9

Changes of the range of motion after facetectomy (°).